

# Moving Beam Helical CT Scanning

Carl R. Crawford,\* *Senior Member IEEE*, Kevin F. King, Thomas L. Toth, and Hui Hu

**Abstract**—Images generated with helical scanning are degraded by partial volume artifacts caused by an increased slice thickness when compared to conventional computed tomography (CT) scanning. The slice thickness for a helical scan is proportional to the sum of the thickness of the fan of radiation and the distance the patient moves during data acquisition. We present a method called moving beam helical scanning (MBHS) which significantly reduces the partial volume artifacts caused by helical scanning. The key element of MBHS is a rotatable collimator that is placed between the X-ray source and the patient. As the patient is translated, the collimator is used to aim the fan on a fixed position in the patient. Once sufficient data are obtained to reconstruct a slice, the collimator is quickly reset to scan a target in the next slice. We examined the performance of MBHS by scanning wires and phantoms on a modified scanner. The full-width-at-tenth-maximum of the slice profile at iso-center for MBHS is identical to conventional CT versus a 59% increase for conventional helical scanning. We conclude that MBHS can be used to obtain the scan rate advantages of helical scanning with image quality comparable to conventional scanning.

## I. INTRODUCTION

COMPUTED tomography (CT) scans of the body are usually acquired in groups while respiration is suspended. An inter-scan delay (ISD) is required between each pair of slices in a group. We define the scan rate of a scanner to be the ratio of the number of scans per group to the time required to collect the slices. Until recently, the scan rate was limited by the ISD as opposed to the data acquisition time itself. During the ISD, the direction of gantry rotation was reversed and the patient translated to the position of the next axial slice. These types of scanners perform what we denote as conventional CT. Present commercially available CT scanners do not reverse direction because of the use of slip rings, which allow for continuous gantry rotation [1]. The ISD can be reduced to zero if the patient is translated simultaneously with data acquisition [2]. The terms *helical*, *volumetric*, and *spiral* scanning have been used to describe the situation with continuous gantry rotation and simultaneous patient translation.

If the data from a helical scan are reconstructed using the conventional filtered backprojection algorithm, the resulting images will be degraded by two effects: the presence of streaks caused by inconsistencies in the projection data and the loss of resolution due to increased partial volume artifacts [3], [4]. There are a number of different methods to minimize the

degradations caused by helical scanning [3], [5]–[9]. The basic differences in the methods are in the amount of data collected and the weighting scheme applied before reconstruction with filtered backprojection. Most of the methods can lower the level of streak artifacts so that they are obscured by quantum noise. However, the partial volume artifacts are still worse than with conventional CT [3], [7], [10].

Yet, there is growing clinical acceptance of helical scanning replacing conventional CT scanning despite the increased partial volume artifacts [11], [12]. One reason for helical scanning's accepted use is that it allows for new scanning protocols. Helical scanning allows for a slice to be reconstructed at any axial position. For example it can center a slice over a lung nodule [13], [14]. The ability to reconstruct overlapping slices improves lesion and nodule detection [15], [16]. In addition, three-dimensional display benefits from having closely spaced slices [17]. Also, helical scanning can generate more slices during the peak enhancement period of a bolus injection of contrast material, allowing for generation of CT angiograms [18]. Because of the partial volume artifacts, helical scanning may not replace all conventional scanning protocols [19]. Reduction of the partial volume artifacts is needed in order that helical scanning be used to replace all conventional CT scanning.

In this paper, we present a method called moving beam helical scanning (MBHS). The key to MBHS is the placement of a rotating collimator between the source and the patient. The collimator is aimed at a fixed point in the patient, called the *target*, while the patient is translated during data acquisition. The collimator has a low moment of inertia so it can be quickly reset to target the next slice. Because the target remains stationary with respect to the X-ray source, conventional CT scanning is emulated and the partial volume artifacts are eliminated at the target. We also show that with the use of this collimator, the partial volume artifacts are significantly reduced for nontargeted points.

In Section II we present a description of MBHS along with a comparison to conventional CT scanning and to conventional helical scanning. Scans of wires and anthropomorphic phantoms on a modified scanner are presented in Section III. Finally, in Section IV we compare MBHS with conventional CT scanning and conventional helical scanning. We also include a discussion of a number of implementation considerations.

## II. METHODS

We first turn our attention to conventional CT scanning and conventional helical scanning. We limit our discussion to third-generation CT scanning. The methods shown here can be extended to fourth and fifth generation CT scanners.

Manuscript received August 9, 1995; revised November 16, 1995. The Associate Editor responsible for coordinating the review of this paper and recommending its publication was G. Gullberg. Asterisk indicates corresponding author.

C. R. Crawford is with Analogic Corp., 8 Centennial Drive, Peabody, MA 01960-7987 USA (e-mail: ccrawford@analogic.com).

K. F. King, T. L. Toth, and H. Hu are with GE Medical Systems, Milwaukee, WI 53201-0414 USA.

Publisher Item Identifier S 0278-0062(96)02530-X.

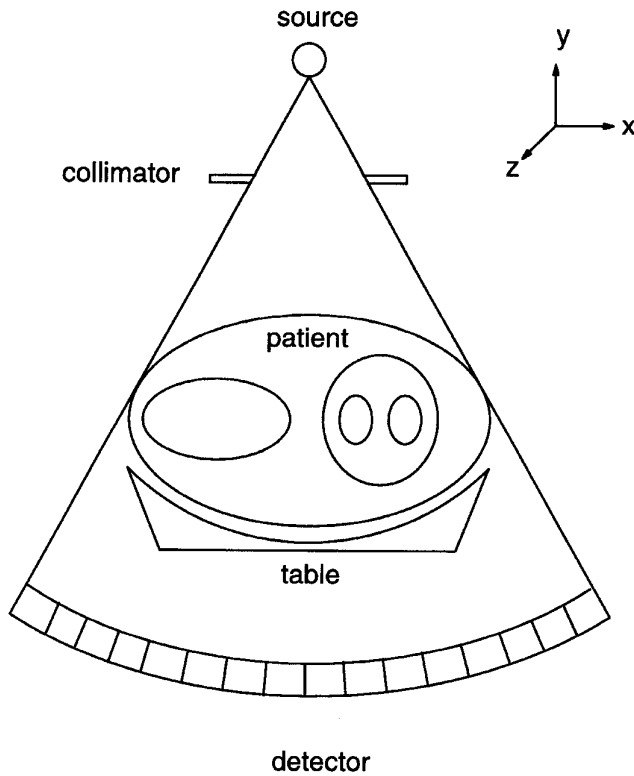


Fig. 1. Front view of a CT scanner showing the key components used in helical scanning. The patient lies on a transportable table. The X-ray source is collimated to form a fan of radiation which is detected by the detector. The detector and source rotate around the  $z$ -axis while the patient is translated along the  $z$ -axis.

Fig. 1 shows a simplified diagram of a patient in a scanner during conventional and helical scanning. The patient lies on a table that can be translated during data acquisition in the axial direction which corresponds to the  $z$ -axis in an  $xyz$ -Cartesian coordinate system. Imaging takes place in the  $xy$ -plane. We use the term constant  $z$ -axis (CZA) to denote conventional CT scanning because the table is kept at a constant  $z$ -location during the scan. For conventional helical scanning, the patient is translated by  $\Delta$ , denoted the displacement distance, during each  $360^\circ$  of gantry rotation. The X-ray source, collimator, and the detector are mounted on a gantry (not shown) that rotates during data acquisition. The source is collimated so that a fan of radiation is allowed to propagate through the patient. A view (or projection) of the patient is the set of detector readings at a given rotational position of the source and the detector.

Next, consider Fig. 2 where we show the side view of the scanner outlined in Fig. 1. In this figure, the source and detector rotate about an axis parallel to the patient. Fig. 2(a) and (b) shows the beginning and ending locations, respectively, of the patient during a helical scan. The pitch of a helical scan is the ratio of displacement distance,  $\Delta$ , to the thickness of the fan. In Fig. 2(b) we can see why partial volume artifacts occur with helical scanning. The lighter shaded region is the cross section of the patient that is irradiated during the scan. The width of this region is the slice thickness for CZA plus the displacement distance,  $\Delta$ . The partial volume artifacts can be reduced by decreasing the pitch.

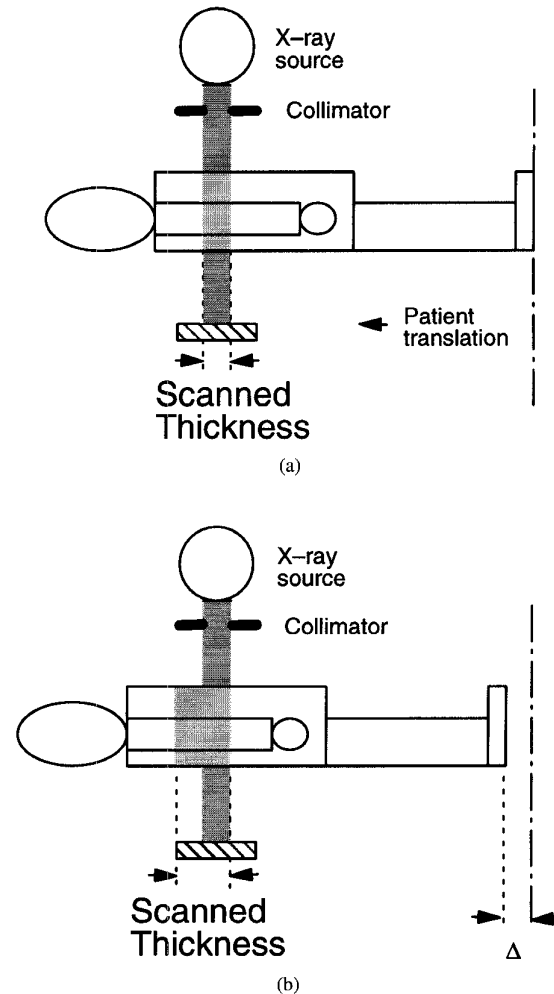


Fig. 2. Side view of the scanner shown in Fig. 1 during helical scanning. The scanner is shown (a) at the beginning and (b) at the end of a helical scan. The lighter shaded region in (a) is the intersection of the fan with the patient at a given rotational position of the gantry. The lighter shaded region in (b) is the total portion of the patient exposed during scanning. The patient moves  $\Delta$ , denoted the displacement distance, during a  $360^\circ$  rotation of the gantry.

However, smaller pitches reduce the scan rate advantages that can be obtained with helical scanning. In this paper, we follow the arguments made by Crawford and King and assume that a unity pitch is optimum [3].

Mori originally suggested that the patient should be translated at a constant speed [2]. We use the term constant speed helical (CSH) to denote this situation. Crawford and King have pointed out that the partial volume artifacts can be reduced by varying the velocity during the course of gantry rotation [3]. We use the term variable speed helical (VSH) to refer to the case when the patient is moved at a variable speed. It has been shown that VSH can be used to reduce, but not eliminate, the partial volume artifacts caused by CSH [3]. In this paper, we refer to both CSH and VSH as conventional helical scanning.

Another point to consider with conventional helical scanning is how the projection data are reconstructed. The various reconstruction techniques acquire projections during multiple  $360^\circ$  rotations of the scanner [3], [5]–[9]. The number of rotations varies from approximately one-half to four. The data

from these sets are interpolated or weighted to compensate for the patient translation that has occurred during data acquisition. Crawford and King concluded that one rotation is optimum when one considers streak artifacts, partial volume artifacts and noise [3]. They concluded that the *underscan* (US) [20] and the helical extrapolative (HE) are the best reconstruction algorithms. All the results in this paper, including those generated with MBHS, were generated with 360 degrees of gantry rotation. The CZA and MBHS scans were reconstructed with underscan. The CSH scans were reconstructed with both US and HE, which are denoted CSH-US and CSH-HE, respectively. MBHS scans were not reconstructed with HE because the target is stationary with respect to the fan and HE compensates for displacement.

Fig. 3 demonstrates how MBHS is implemented. The figure is identical to Fig. 2 with the exception that the collimator has the ability to translate, relative to the source, during data acquisition. The translational capability of the collimator is used to keep the fan positioned on the target in the patient. The lighter shaded region in Fig. 3(b) is the cross section of the patient that is radiated with MBHS. When one compares this region to the corresponding region in Fig. 2(b), it is seen that the partial volume artifacts will be less with MBHS at the targeted point. Elsewhere, the partial volume artifacts will be a function of the scanner's geometry. The detector has to have sufficient axial extent so that the projected fan is detected.

We implemented MBHS on a modified 9800 Hilight Scanner (GE Medical Systems, Milwaukee, WI). The collimator that we used is diagramed in Fig. 4. The key element of the collimator is a rotatable mandrel with a V-shaped slot. Instead of translating a collimator as described above, the mandrel is rotated as shown in Fig. 5. The slot is cut so that the thickness of the fan is determined by the width of the slot at the point that the radiation exits the collimator. Because the mandrel has a low moment of inertia, it can be rotated quickly and set to target the next slice after the completion of a slice in less than 20 msec. In our implementation, the detector had sufficient axial extent to intersect the fan for all mandrel positions for slice thicknesses up to approximately 7 mm.

The angular position of the collimator was controlled with a micro-computer (PC). The axial position and velocity of the table were controlled by an external power supply. The PC was synchronized with the scanner via a signal which indicates that X-rays were on. All scanning was done with two second scan times and 5 mm thick slices. The scanner's source-to-collimator, source-to-center, and source-to-detector distances are 250 mm, 630 mm, and 1100 mm, respectively. The elements of the detector are on a 1-mm spacing. The computer and external power supply could also be set up to obtain CZA and CSH scans. For CZA and CSH, the collimator was not rotated. In the case of CZA, the table was also kept stationary. We performed two experiments to evaluate the performance of MBHS relative to CZA and CSH. The two areas of interest are the slice profile and structured artifacts because these differentiate helical from conventional scanning [3].

The slice profile is defined to be the response to small objects at various displacements parallel to the  $z$ -axis [21].

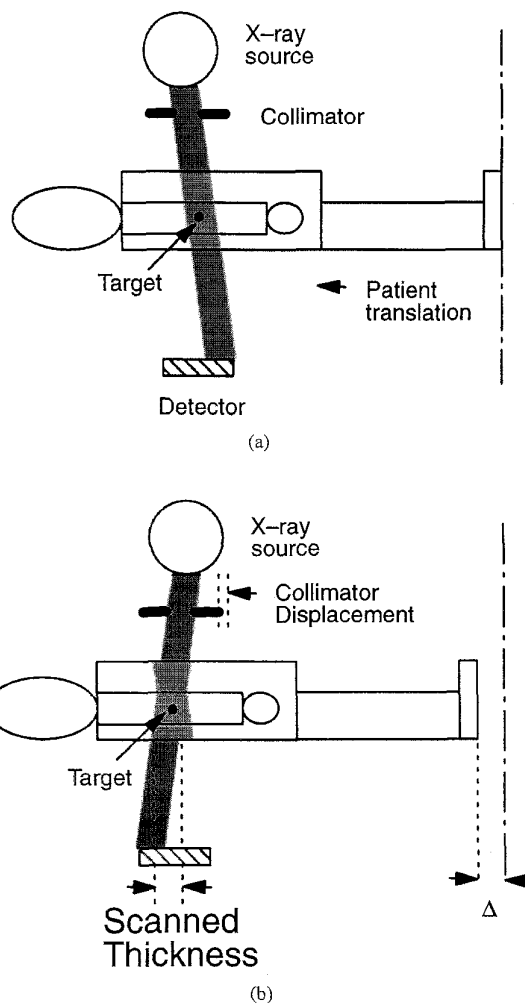


Fig. 3. Side view of the scanner during MBHS. The collimator is positioned during the scan to target a fixed point in the patient. The portion of the patient exposed to radiation, the lighter shaded region in (b), is less than the case shown in Fig. 2(b).

Slice profiles for helical scanning have been measured using small aluminum disks that represent impulse functions [7] and using thermoluminescence dosimeter (TLD) measurements [22]. We want to measure the slice profile at various positions in the field-of-view because the slice profile is a function of the radial distance from the iso-center of the scanner. We also want to compare MBHS to CZA and CSH. Therefore, the use of small objects to measure the slice profile would be prohibitively time consuming. In order to measure the slice profile, we scanned a tungsten wire (.25-mm diameter) which was tilted  $22.5^\circ$  with respect to the slice plane. The use of wires follows from the measurement of the slice profile using an aluminum wedge [21]. The slice profiles can be obtained by projecting the maximum absolute values of the reconstructions of the wire onto either the horizontal or vertical axes depending on the orientation of the wire. The projections have to be scaled to compensate for the wire being at  $22.5^\circ$ . The slice profile measurements are affected by the spatial-dependent point spread function (PSF) of the scanner [23], [24]. However, it has been argued that the effect of the PSF on the measurement

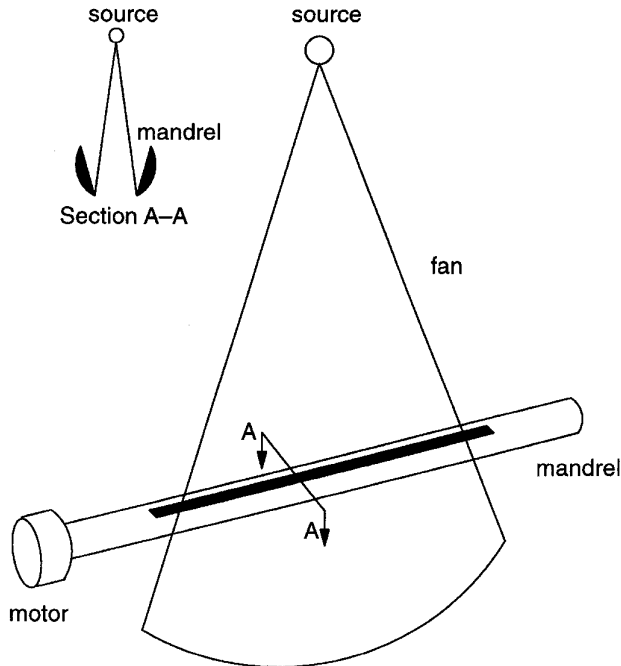


Fig. 4. Detailed drawing of the collimator used in MBHS. The key component is the mandrel which is rotated by the motor during the course of the scan.

of the slice profile is small [21]. In the discussion of the results presented below, all comparisons are made relative to CZA at the same place in the field-of-view. Therefore, the PSF should not affect the comparison of the algorithms. Because the profiles for CSH are not generally rectangular [3], we use the values of the full-width-at-half-maximum (FWHM) and the full-width-at-tenth-maximum (FWTM) as measures of the slice profile. We suspect that the FWHM and FWTM are not necessarily meaningful measures of the effective slice width because the slice profiles are irregular. We present the measures because they are traditionally used.

Three phantoms were scanned with CZA, CSH, and MBHS. The CZA data were reconstructed without any projection weighting, which is denoted as *fullscan* (FS) [3]. The CSH data were reconstructed with underscan and with the helical extrapolative algorithm according to the CSH-US and CSH-HE methods, respectively. Finally, the MBHS data were reconstructed with underscan. All data were obtained with the same scanning techniques (tube potential, tube current, and scan time). The scans were obtained with 5-mm slice thicknesses. When helical data were collected with MBHS and CSH, a helical pitch of one was used. The data were reconstructed with a stand-alone reconstruction package because software present on the scanner did not support helical extrapolative.

The three phantoms simulated the head, body (abdomen and lung), and the spine. The head phantom is the Tommy Computerized Tomography Phantom (Nuclear Associates, 100 Voice Road, Carle Place, NY) and consists of a natural human skull filled with tissue-equivalent material. The body phantom is the Alderson Humanoid (Alderson Research Laboratories, 390 Ludlow Street, Stamford, CT) and consists of real human

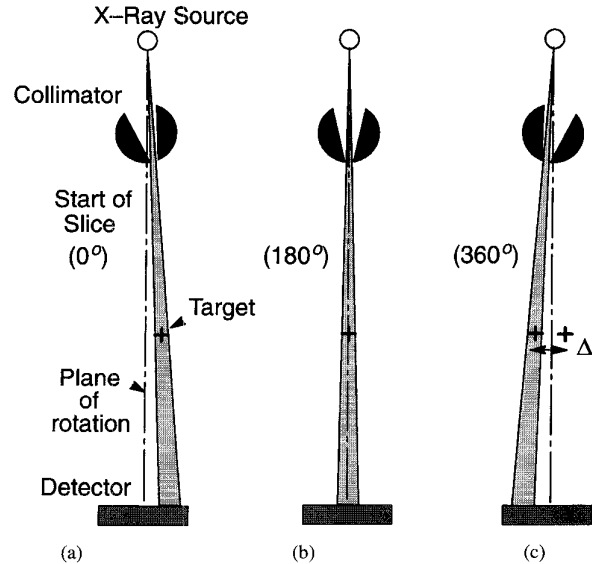


Fig. 5. The mandrel with the v-shaped slot is used to target the fan on a fixed point in the patient at the (a) beginning, (b) middle, and (c) end of the scan. The target is indicated with a plus sign (+).

TABLE I  
THE FWHM AND FWTM OF THE SLICE PROFILE AT DIFFERENT POSITIONS IN THE FIELD-OF-VIEW FOR CZA, CSH, AND MBHS. THE VALUES WERE CALCULATED FROM THE SLICE PROFILES, SOME OF WHICH ARE SHOWN IN FIG. 6. THE COORDINATE SYSTEM,  $(x, y)$ , IS SHOWN IN FIG. 1

X (mm)	Y (mm)	CZA		CSH-US		CSH-HE		MBHS	
		FWHM	FWTM	FWHM	FWTM	FWHM	FWTM	FWHM	FWTM
0	0	5.1	5.8	5.0	9.0	5.2	8.4	5.1	5.8
-200	0	3.9	5.7	3.8	8.7	4.1	7.4	4.0	6.1
-100	0	4.7	5.6	4.4	8.6	4.5	8.0	4.7	5.5
100	0	4.6	5.6	4.4	8.9	4.5	8.0	4.6	5.8
200	0	4.1	6.0	3.9	8.7	4.0	7.9	4.2	6.2
0	-200	4.6	6.4	6.9	8.4	6.7	8.4	4.9	6.8
0	-100	5.1	6.2	5.9	8.9	5.9	8.5	5.2	6.2
0	100	4.5	6.1	4.2	9.1	4.5	7.9	4.5	6.0
0	200	3.9	5.9	3.7	8.6	3.7	6.6	3.8	6.0

bone and tissue equivalent material. The spine phantom is a real human spine in a plexiglass cylinder filled with water.

The phantom scans were reviewed by three radiologists, who were asked to rank the images by relative image quality. The images were not annotated, and the physicians were not told which images were which until after the review was completed. Two of the radiologists reviewed the images on film. The third radiologist reviewed the images on a workstation.

### III. RESULTS

The slice profiles for the wire scans are shown in Fig. 6 and the corresponding values of the FWHM and FWTM are listed in Table I. From the table it is seen that helical scanning has the greatest effect on the FWTM. For CSH-US, the FWTM increases relative to CZA, 59% at the center, and between 31 and 59% depending on where the wire is located away from the center. For CSH-HE, a 45% increase was measured at iso-center and between 12 and 45% elsewhere in the field-of-view. For MBHS, the FWTM was the same as CZA at iso-center and increased up to 7% 200 mm away from iso-center. For all practical purposes, we conclude that the slice profiles for MBHS and CZA are identical.

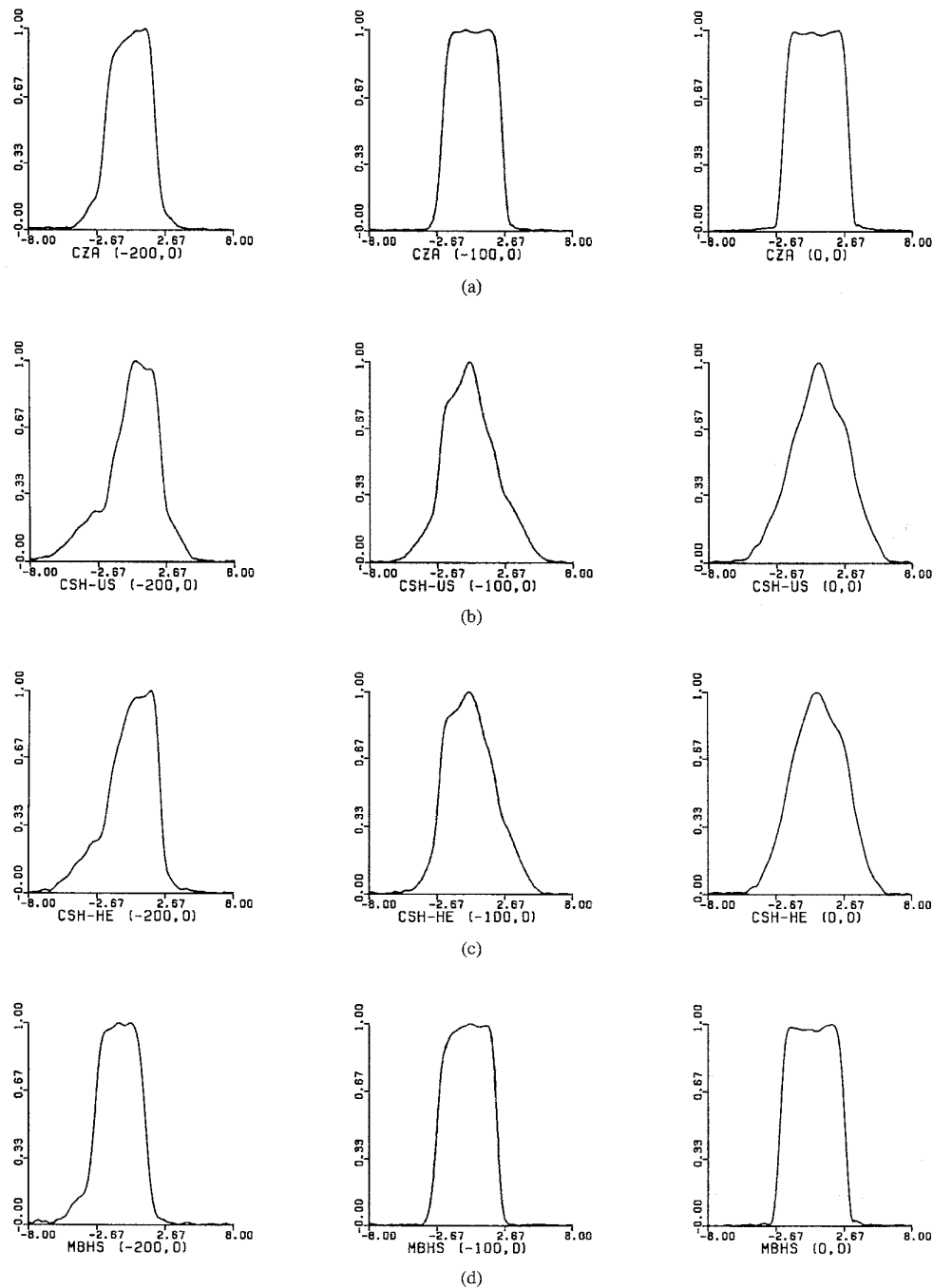


Fig. 6. Slice profiles at different positions in the field-of-view for (a) CZA, (b) CSH-US, (c) CSH-HE, and (d) MBHS, calculated from 5-mm wire scans. The spatial locations, which are indicated by  $(x, y)$  below the horizontal axes, correspond to the coordinate system shown in Fig. 1. The units on the horizontal axes are millimeters. The units on the vertical axes are arbitrary.

Three other effects can be discerned in the table and in Fig. 6. The first effect is that the FWHM gets narrower away from center for CZA, CSH, and MBHS. The narrowing can be understood by examining the data collection and reconstruction processes. The source has a shorter axial extent than does the detector. As a result, the fan is thinner when an object is closer to the source. The reconstruction algorithm for fan-beam projections weights points closer to the source

more than points nearer the detector [25]. As one moves away from the center, the reconstruction algorithm will give greater weight to contributions where the fan is thinner and thus the slice profile will be narrower. The second effect is that the results are fairly symmetric along the  $x$ -axis but not along the  $y$ -axis. This effect is due to the fact that the initial position of the source is along the  $y$ -axis and due to the projection modulation caused by projection weighting. The third effect

is that there are some minor modulations and asymmetries in the slice profiles due to, we suspect, aliasing [26] and the exponential edge-gradient effect [27].

Our second experiment was to scan three anthropomorphic phantoms. We do not present the images in this paper because the differences are subtle and can only be seen on film or using a workstation. The head scans demonstrate that CSH-US has a number of black and white streaks in the posterior fossa. The MBHS, CSH-HE, and CZA results are virtually identical to an untrained eye. No additional structured artifacts are seen in the MBHS image.

The physicians ranked CSH-US as the most inferior method because of the presence of streaks and shading artifacts. After comparing a number of structures, they unanimously determined that CSH-HE was the next best. They had trouble choosing between MBHS and CZA. In general, they found that CZA better than MBHS. However, in a few cases (physician/phantom) MBHS was judged to be better than CZA.

#### IV. DISCUSSION

The fundamental problem with conventional helical scanning (CSH and VSH) is that the patient is moving axially with respect to the fan during data collection. The effect of the movement is to generate partial volume artifacts in helical scans. Clinical feedback has indicated that CSH cannot always be used as a direct replacement for conventional scanning. There are times, however, that the increased scan rate of helical scanning can be traded off for the increased partial volume artifacts. VSH could be used to practically eliminate the artifacts. However, it might be difficult to design a control system that synchronizes the axial position of the patient with the angular position of the source for VSH. Additionally, VSH could induce motion sickness. We have shown in the previous section that MBHS has a slice profile comparable to conventional scanning and that no structured artifacts are generated. Therefore, MBHS has the potential to replace conventional scanning and obtain the scan rate advantages of conventional helical scanning.

An assumption made in Section II was that the detector has to have sufficient axial extent to capture the fan at all positions of the collimator. In our system, the detector could only support MBHS with slices up to about 7 mm thick. Clinical feedback has indicated that if the images generated with helical scanning were comparable to conventional scanning, then 5-mm slices would be used routinely. If thicker slices are required, however, the detector could be redesigned to increase its axial extent. Another alternative is to stop tracking the target when the penumbra of the fan projects beyond the ends of the detector. A result of this alternative is that the partial volume artifacts would increase. Another method to deal with the finite axial extent of the detector is to move the collimator so that the beam tracks at a constant speed during data acquisition, where the speed is less than the speed required to track a fixed point. Computer simulations have shown that tracking at a slower speed is better than stopping the collimator and better than CSH-HE.

The response of the detectors used in our system varies as a function of the axial position of the fan. In conventional

scanning, we detect the position of the fan and use software to correct for the detector response [28]. We have found that the correction was not robust enough to handle the displacement of the fan caused by MBHS and rings were introduced into the images because of fixed errors in the projections [29]. We improved the correction by collecting calibration scans at a number of different rotational positions of the collimator.

The results shown in the previous section were generated with the center-of-rotation of the scanner being the target of the collimator. The results show that the slice profile was almost equivalent to CZA even for points up to 200 mm away from the center. Additional reduction in the partial volume artifacts for off-center objects could be obtained by focusing the fan on a specific point of interest.

The radiologists had some complaints about the phantom study. The first complaint was that the slices were obtained at slightly different axial positions. We estimate that there was about 0.1–0.2 mm of slice separation due to errors in our experimental process. The ranking process was complicated because the differences in the location of the slices, particularly in the bone, had to be factored out. The second complaint was that phantoms were used instead of patients or volunteers. The phantoms were deficient in modeling actual human cross-sectional anatomy, particularly in the soft tissue structures. We are not presently able to scan volunteers on the modified scanner because the modifications render the scanner unsafe. Furthermore, it would be extremely difficult to coordinate a patient's respiration so that similar scans of the body could be obtained. We are not sure why sometimes the MBHS images were ranked above the CZA images. Two reasons come to mind and need further validation. The first is that underscan was used for MBHS and fullscan for CZA. Perhaps underscan is useful in cases when motion is not present or when the increased noise in underscan masks artifacts in the fullscan reconstruction. A full discussion of the dose tradeoffs of the various reconstruction algorithms can be found in [3]. The second reason is that perhaps the modifications to the mandrel, which were made to support MBHS, caused a degradation in CZA scans.

The MBHS reconstructions shown in the previous section were generated with the underscan algorithm. Underscan was originally developed to reduce artifacts caused by patient motion. The main problem with motion is that the first and last views in a scan are effectively acquired from two different objects. As a result, streaks are generated toward the initial position of the source. Underscan exploits the fact that there are actually two sufficient sets of projections present in a 360 degree scan. The projections at the beginning and end of the scans are contained in the first set of projections and are attenuated. Corresponding projections in the second set of projections are amplified to compensate for the attenuation of the projections in the first set. Crawford and King demonstrated that underscan is also effective in removing the structured artifacts caused by CSH and VSH [3]. We found that MBHS generates structured artifacts in the vicinity of dense objects, like bones, that were far from the targeted position. We also found that underscan was effective in removing these artifacts.

Another advantage of MBHS is that high resolution CT (HRCT) is permitted. HRCT requires the interleaving of the two sets of projections found in a  $360^\circ$  scan to reduce aliasing [30]. When HRCT is used in conjunction with underscan, the projection attenuation makes the interleaved projections unequal, resulting in increased aliasing. For objects near the center, MBHS requires no underscan weighting to eliminate structured artifacts, enabling alias-free HRCT. For off-centered targets, alias-free HRCT can be traded for a small amount of structured artifacts by turning off underscan. The artifact is small relative to CSH without underscan. Alternatively, the fan could be focused on the specific region of interest.

Crawford and King demonstrated [3] that the *halfscan* reconstruction algorithm [31] is also effective in removing structured artifacts caused by CSH. We have found that halfscan also removes the artifacts caused by MBHS. This conclusion was reached by scanning anthropomorphic phantoms with a unity pitch. A disadvantage of halfscan reconstructions is increased noise and the necessity to increase the pitch to approximately 1.7 so that the slices are contiguous. Preliminary scans have shown that no significant additional structured artifacts are generated with the larger pitch.

Throughout this paper, we have referred to the fan as having a certain thickness. In practice, the profile of the fan would have a trapezoidal cross section due to the presence of an umbra and penumbra in the radiation that reaches the detector. When we quoted slice thicknesses above, we were referring to the FWHM of the slice profile. The mandrel that is present in the rotating collimator was not designed with the umbra and penumbra in mind. It might be possible to improve the slice profile results shown in the previous section with a better designed mandrel. Some commercial CT scanners have a collimator between the patient and the detector, called a post-patient collimator, to block some of the penumbra from reaching the detector. (The 9800 Hilight scanner that we used in our experiments did not have a post-patient collimator.) MBHS will be more difficult to implement in this case because the post-patient collimator will have to be moved as the fan is moved using the rotating collimator. The mandrel that we used caused the slice thickness to change as a function of its rotational position.

A problem with MBHS is that the collimator must be quickly repositioned at the end of each rotation. Data acquired during the repositioning will degrade the slice profile. Conversely, if data are not acquired during this time, the source must be turned off or else the patient will be subjected to needless radiation. In our case, the collimator could be reset in about 20 msec, and we suspect that we can ignore the movement during data acquisition because the projections acquired during that time are attenuated by the underscan algorithm. If the attenuation proves to be insufficient, the underscan algorithm can be modified to eliminate the contributions of these projections altogether. If in an implementation of MBHS the collimator cannot be reset quickly, the collimator width could be ramped to zero at the beginning and end of the scans. This allows the collimator and source to be repositioned as quickly as is practical without changing the current delivered by the generator. If the collimator width is to be changed as

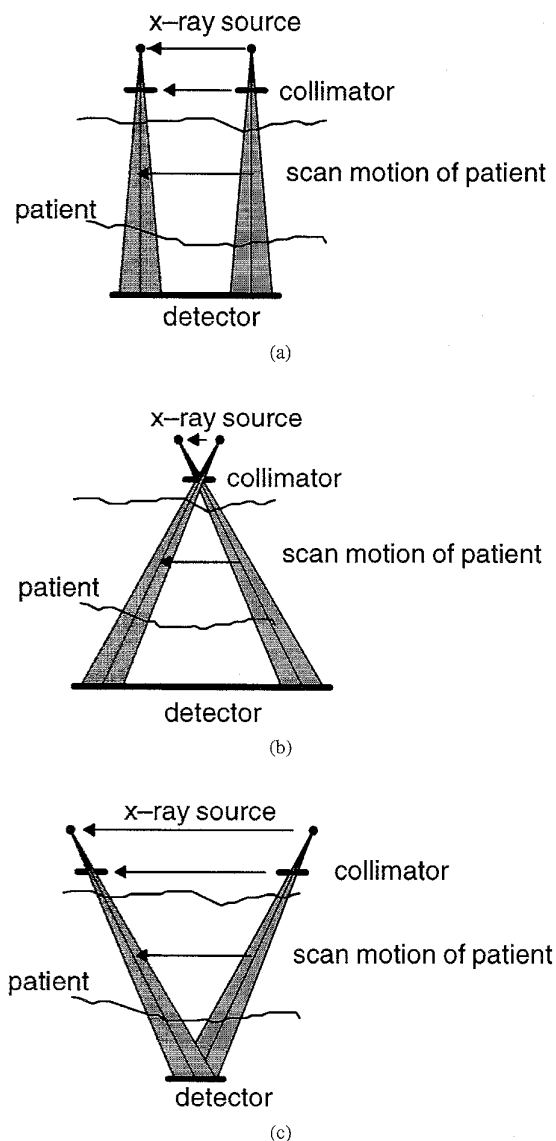


Fig. 7. Variations of MBHS: (a) both the source and the collimator are displaced, (b) only the source is moved, and (c) the source and the collimator are moved at different rates so that the fan remains stationary on the detector. Note that the aspect ratios of the drawings have been exaggerated to emphasize the key elements of these variations.

well as its position, the collimator will probably have to consist of two moving blades. Another way to account for the time required to reset the source and/or the collimator is to slow the translational speed of the patient during the time it takes to perform the reset. If the table speed is reduced, then MBHS will suffer the same disadvantages of VSH.

We have demonstrated that a given position in the patient, called the target, can be kept fixed with respect to the fan using a rotating collimator. As indicated above, there are a few problems with this method. The method demands a detector with larger axial extent and a detector with a very linear response over its length. Also, the method only targets one point in the patient. We now present a number of variations to MBHS that overcome some or all of these problems.

A variation of MBHS that completely eliminates the slice profile degradation is obtained by moving both the X-ray source and collimator synchronously with the patient and at the same rate so that rays in the same plane through the patient are intercepted by the detector throughout the scan. This variation is illustrated in Fig. 7(a). This variation has the advantage of having image quality equal to conventional scanning. It has the disadvantages of requiring both the collimator and X-ray source to reset their starting positions and also that the X-ray beam position changes greatly on the detector during the scan, requiring a robust detector calibration method. The rapid motion of the X-ray source could be accomplished by using sources that support their rotating anodes with magnetic bearings [32], [33]. It is not clear, however, if it would be practical to use magnetic bearings to achieve the displacement required for MBHS. Baer *et al.* have also described a method which is similar to this variation of MBHS [34]. They describe a system in which the source, collimator and detector are mounted on a carrier that can be axially offset from the gantry. We suspect that it would not be practical to reset the carrier fast enough to achieve an increase in scan rate of the scanner.

Another variation of MBHS reduces the data inconsistency by moving the source synchronously with the patient while keeping the collimator fixed such that the detector always intercepts a ray from the source through the target. This variation is illustrated in Fig. 7(b). It has the advantage of requiring the motion and rapid reset of only the source and not the collimator. This is an advantage because the source may be moved more quickly than the collimator by magnetic bearing steering of the anode. Also, the source has to be moved less than with the previous variation. The method still suffers the disadvantage of a moving X-ray beam on the detector and thus requiring a robust detector calibration method. This variation and the previous variation might be more susceptible to scatter because of the increased axial extent of the detector versus conventional scanning.

The final variation of MBHS also reduces the data inconsistency by moving the X-ray source and collimator synchronously with the patient. However, the X-ray source and collimator move at different speeds in such a way as to keep the position of the X-ray beam fixed on the detector thus averting one of the disadvantages of the previous variations. This variation is shown in Fig. 7(c). Note that in this variation, the partial volume degradation is reduced relative to conventional helical scanning, because the magnification factor of the target is smaller, but not completely eliminated as with the first variation.

A drawback of MBHS is that it does not allow the reconstruction of slices at arbitrary axial positions, which is useful to center a slice on a nodule or to improve the quality of surface displays and reformations. A scanner that performs MBHS, however, can be made into a conventional helical scanner by just turning off the control of the moving beam when slices at arbitrary positions are required.

The phantom scanning shows that CSH-HE generates fewer artifacts than CSH-US, particularly in regions where dense objects, such as bone, have rapid density changes in the axial direction. Crawford and King recommended that CSH-

US be used because underscan might be implemented on a conventional scanner [3]. However, their results were based on limited trials of helical scanning and the results in this paper support the effort required to implement CSH-HE.

In conclusion, we have shown a method called MBHS that significantly reduces the partial volume artifacts present in conventional helical scanning methods. The key to MBHS is the use of a rotatable collimator that focuses the fan of radiation from the source on a fixed point in the patient. We have used scans on a modified scanner to demonstrate the potential of MBHS. The slice profile of MBHS is comparable to conventional scanning and it appears that no additional artifacts are generated. Additional trials will be required to completely determine the clinical benefits of MBHS.

#### ACKNOWLEDGMENT

The authors acknowledge the following. E. Curry, M. Gard, W. Hampel, and M. Limkeman modified the commercial scanner so that MBHS data could be collected. K. Baxter, S. Fox, R. Kinsinger, G. Seidenschur, and B. Senzig provided insights on the clinical and technical aspects of helical scanning. D. Birzer, L. Carter, and O. Dake provided software tools that were used to reconstruct images and display images. Information about the use of magnetic bearings for rotating-anode X-ray tubes was provided by G. Carlson, B. Lounsbury, and J. Newman. G. Besson, J. Hsieh, H. Levy, A. Pfoh, and J. Sandrik provided suggestions during their reading of the manuscript. W. D. Foley, J. D. Godwin, and R. Starshak reviewed the phantom images. C. Ritchie strengthened the content of the paper through his careful reviews and facilitated the transfer of the phantom images to a workstation. D. Jacobson provided details on the construction of the spine phantom.

#### REFERENCES

- [1] K. L. Dinwiddie, R. G. Friday, J. A. Racz, and E. J. Seppi, "Tomographic scanning apparatus," U.S. Patent 5 093 850, 1992.
- [2] I. Mori, "Computerized tomographic apparatus utilizing a radiation source," U.S. Patent 4 630 202, 1986.
- [3] C. R. Crawford and K. F. King, "Computed tomography scanning with simultaneous patient translation," *Med. Phys.*, vol. 17, pp. 967-982, 1990.
- [4] G. Wang and M. W. Vannier, "Longitudinal resolution in volumetric X-ray computerized tomography-analytic comparison between conventional and helical computerized tomography," *Med. Phys.*, vol. 21, pp. 429-433, 1994.
- [5] H. Nishimura and O. Miyazaki, "CT system for spirally scanning subject on a movable bed synchronized to X-ray tube revolution," U.S. Patent 4 789 929, 1988.
- [6] Y. Bresler and C. J. Skrabacz, "Optimal interpolation in helical scan computed tomography," in *Proc. ICASSP*, Glasgow, Scotland, 1989, pp. 1472-1475.
- [7] W. A. Kalender and A. Polacin, "Physical performance characteristics of spiral CT scanning," *Med. Phys.*, vol. 18, pp. 910-915, 1991.
- [8] T. Katakura, K. Kimura, S. Midorikawa, N. Hashimoto, and K. Suzuki, "Improvement of resolution along patient axis in helical-volume CT," *Radiol.*, vol. 177P, p. 108, 1990.
- [9] W. A. Kalender, W. Seissler, E. Klotz, and P. Vock, "Spiral volumetric CT with single-breath-hold technique, continuous transport, and continuous scanner rotation," *Radiol.*, vol. 176, pp. 181-183, 1990.
- [10] H. Rigauts, G. Marchal, A. L. Baert, and R. Hupke, "Initial experience with volume CT scanning," *J. Comput. Assist. Tomogr.*, vol. 14, pp. 675-682, 1990.
- [11] D. A. Bluemke and E. K. Fishman, "Spiral CT of the liver," *AJR*, vol. 160, pp. 787-792, 1993.



- [12] R. K. Zeman, A. S. Zeiberg, W. J. Davros, S. M. Ascher, C. J. Cooper, D. I. Weltman, R. Patt, B. S. Garra, D. L. Griego, and P. M. Silverman, "Routine helical CT of the abdomen: Image quality considerations," *Radiol.*, vol. 189, pp. 395-400, 1993.
- [13] P. Vock, M. Soucek, M. Daepf, and W. A. Kalender, "Lung: Spiral volumetric CT with single-breath-hold technique," *Radiol.*, vol. 176, pp. 864-867, 1990.
- [14] P. Costello, W. Anderson, and D. Blume, "Pulmonary nodule: Evaluation with spiral volumetric CT," *Radiol.*, vol. 179, pp. 875-876, 1991.
- [15] B. A. Urban, E. K. Fishman, J. E. Kuhlman, A. Kawashima, J. G. Hennessey, and S. S. Siegelman, "Detection of focal hepatic lesions with spiral CT: Comparison of 4- and 8-mm interscan spacing," *AJR*, vol. 160, pp. 783-785, 1993.
- [16] W. A. Kalender, A. Polacin, and C. Suss, "A comparison of conventional and spiral CT: An experimental study of the detection of spherical lesions," *J. Comput. Assist. Tomogr.*, vol. 18, pp. 167-176, 1994.
- [17] S. Aoki, Y. Sasaki, T. Machida, T. Ohkubo, M. Minami, and Y. Sasaki, "Cerebral aneurysms: Detection and delineation using 3-D-CT angiography," *AJNR*, vol. 13, pp. 1115-1120, 1992.
- [18] S. Napel, M. P. Marks, G. D. Rubin, M. D. Dake, C. H. McDonnell, S. M. Song, D. R. Enzmann, and R. B. Jeffrey, "CT Angiography with spiral CT and maximum intensity projections," *Radiol.*, vol. 185, pp. 607-610, 1992.
- [19] B. R. Herts, D. M. Einstein, and D. M. Paushter, "Spiral CT of the abdomen: Artifacts and potential pitfalls," *AJR*, vol. 161, pp. 1185-1190, 1993.
- [20] N. J. Pelc and G. H. Glover, "Method for reducing image artifacts due to projection measurement inconsistencies," U.S. Patent 4 580 219, 1986.
- [21] R. A. Brooks and G. DiChiro, "Slice geometry in computer assisted tomography," *J. Comput. Assist. Tomogr.*, vol. 1, pp. 191-199, 1977.
- [22] K. A. Jerjian, B. I. Goshorn, R. E. Hendrick, B. R. Westerman, and D. Thickman, "Performance evaluation of helical volumetric CT scanning," *Radiol.*, vol. 181P, p. 111, 1991.
- [23] G. Schwierz, W. Lichtenberg, and K. Fuhrer, "Influence of the focal spot on CT image quality," *Electromed.*, vol. 4, pp. 134-139, 1980.
- [24] C. R. Crawford and N. J. Pelc, "Angular integration and inter-projection correlation effects in CT reconstructions," in *Proc. IEEE Eng. Medicine Biol. Soc.*, 1987, vol. 9, pp. 1670-1671.
- [25] A. C. Kak and M. Slaney, in *Principles of Computerized Tomographic Imaging*. Piscataway, NJ: IEEE Press, 1987.
- [26] C. R. Crawford and A. C. Kak, "Aliasing artifacts in computerized tomography," *Appl. Opt.*, vol. 18, pp. 3704-3711, 1979.
- [27] P. M. Joseph and R. D. Spital, "The exponential edge-gradient effect in X-ray computed tomography," *Phys. Med. Biol.*, vol. 26, pp. 473-487, 1981.
- [28] G. H. Glover and E. M. Kerwin, "X-ray detector with compensation for height-dependent sensitivity and method of using same," U.S. Patent 4 559 639, 1985.
- [29] G. Kowalski, "The influence of fixed errors of a detector array on the reconstruction of objects from their projections," *IEEE Trans. Nucl. Sci.*, vol. NS-24, pp. 2006-2016, 1977.
- [30] N. J. Pelc, G. H. Glover, and T. R. Griffie, "A higher resolution fan-beam reconstruction algorithm for rotate-rotate CT systems," *J. Comput. Assist. Tomogr.*, vol. 4, p. 715, 1980.
- [31] D. L. Parker, "Optimal short scan convolution reconstruction for fan-beam CT," *Med. Phys.*, vol. 9, pp. 254-257, 1982.
- [32] G. A. Cornelissen, H. J. Gerrits, and E. M. Kamerbeek, "X-ray tube having a magnetically supported rotary anode," U.S. Patent 4 322 624, 1982.
- [33] H. Sudo and A. Takahashi, "Rotary anode X-ray tube," European Patent application 0 071 456, 1982.
- [34] U. Baer, W. Distler, and P. Grassmann, "Radiation diagnostic apparatus," U.S. Patent 4 426 715, 1984.